IOP Publishing Journal of Physics: Condensed Matter
J. Phys.: Condens. Matter **21** (2009) 424116 (9pp) doi:10.1088/0953-8984/21/42/424116

Dynamics of binary mixtures with ions: dynamic structure factor and mesophase formation

Takeaki Araki and Akira Onuki

Department of Physics, Kyoto University, Kyoto 606-8502, Japan

Received 24 April 2009, in final form 28 July 2009
Published 29 September 2009
Online at stacks.iop.org/JPhysCM/21/424116

Abstract
Dynamic equations are presented for polar binary mixtures containing ions in the presence of preferential solvation. In one-phase states, we calculate the dynamic structure factor of the composition accounting for ion motion. Microphase separation can take place for sufficiently large solvation asymmetry of the cations and the anions. We show two-dimensional simulation results of the mesophase formation with an antagonistic salt, where the cations are hydrophilic and the anions are hydrophobic. The structure factor $S(q)$ in the resultant mesophase has a sharp peak at an intermediate wavenumber of the order of the Debye–Hückel wavenumber. As the quench depth is increased, the surface tension nearly vanishes in mesophases due to an electric double layer.

(Some figures in this article are in colour only in the electronic version)

1. Introduction

Much attention has been paid to the phase transition behavior arising from the Coulomb interaction among charged particles in various soft materials including electrolytes, polyelectrolytes, and gels [1–3]. However, in most of the theoretical literature, the ion–dipole interaction has not been explicitly considered, which gives rise to a complex structure around each ion, called the solvation (hydration) shell, composed of several solvent molecules (those of the more polar component in a mixture solvent) [4]. The resultant solvation chemical potential $\mu_{\rm sol}^{j}$ depends on the ion species j and typically exceeds the thermal energy T. It should also strongly depend on the composition for binary mixtures and the polymer volume fraction for polymer solutions, so it cannot be neglected at phase transitions and around composition heterogeneities. Recently, including the preferential solvation effect, several theoretical groups have begun to investigate the ion effects in electrolytes [5–9], polyelectrolytes [10], and ionic surfactants [11].

We mention some experiments directly related to our theory. First, many authors have long observed salt-induced phase separation or homogeneization in aqueous binary mixtures, where the phase behavior is strongly altered even by a small amount of a salt [12]. Second, we mention a number of observations of salt-induced aggregates in near-critical binary mixtures [13–15], where the cations and anions are both hydrophilic. In one-phase states [13, 14], heterogeneities extending over a few micrometers have been detected by light scattering with addition of a salt (for example, 17 mass% NaBr in mixtures of H_2O + 3-methylpyridine (3MP) [14]). In a two-phase state [15], a macroscopic thin plate has been observed at a liquid–liquid interface, which presumably consists of aggregates of solvated ions. Third, we mention recent small-angle neutron scattering experiments by Sadakane *et al* [16, 17]. They added sodium tetraphenylborate $NaBPh_4$ at 100 mM to a mixture of D_2O and 3MP to find a peak at an intermediate wavenumber q_m ($\sim$0.1 Å^{-1}). The peak height of the SANS intensity was much enhanced with the formation of periodic structures. Their salt is composed of hydrophilic Na^+ and hydrophobic BPh_4^-. Furthermore, the mixture exhibited colors changing dramatically on approaching the criticality at low salt content ($\sim$10 mM).

Hydrophilic and hydrophobic ions interact differently with the composition fluctuations in mixtures of water + less-polar component. They behave antagonistically in the presence of the composition fluctuations. We may predict the formation of a large electric double layer at liquid–liquid interfaces much reducing the surface tension and formation of mesophases for sufficiently large solvation asymmetry [5, 6]. However, we do not know the details of the phase transition of binary mixtures with an antagonistic salt. Originally, Nabutovskii *et al*

[18] pointed out the possibility of mesophases in electrolytes assuming a coupling between the composition and the charge density in the free energy.

In section 2, we will present a short summary of the statics of binary mixtures containing ions accounting for the preferential solvation. In section 3, dynamic equations for such systems will be given and, as an application, the dynamic scattering amplitude will be calculated. In section 4, we will then numerically examine the mesophase formation induced by antagonistic ion pairs.

2. Ginzburg–Landau free energy

2.1. Electrostatic and solvation interactions

We consider a polar binary mixture containing a small amount of salt. The composition of a water-like component is written as ϕ. The cation and anion densities are written as n_1 and n_2 with charges Z_1e and Z_2e. In the monovalent case we have $Z_1 = 1$ and $Z_2 = -1$. They are sufficiently dilute and their volume fraction is negligible. The charge density is given by $e(Z_1n_1 + Z_2n_2)$. The variables ϕ, n_1, and n_2 vary smoothly in space. The Boltzmann constant will be set equal to unity. As the geometry of our system, our fluid is between parallel metallic plates in the region $0 < z < L$. The lateral dimensions in the xy plane are much larger than L. The surface charges on the plates can give rise to an applied electric field. In the following theory, we fix the charges on the plates such that their electrostatic energy is kept fixed [19].

The Ginzburg–Landau free energy functional of our system is written as $F = \int \mathrm{d}\boldsymbol{r} f$ with the free energy density [5, 6],

$$f = f_0(\phi, T) + \frac{TC}{2}|\nabla\phi|^2 + \frac{\varepsilon \boldsymbol{E}^2}{8\pi} + T\sum_j [\ln(n_j v_0) - 1 - g_j\phi]n_j. \tag{2.1}$$

The first two terms constitute the usual Ginzburg–Landau free energy density. The chemical part $f_0 = f_0(\phi, T)$ depends on ϕ and T and the coefficient C of the gradient term is of the order a^{2-d} in d dimensions, where a is the molecular radius. The third term is the electrostatic free energy, where $\boldsymbol{E} = -\nabla\Phi$ is the electric field and the electrostatic potential Φ satisfies the Poisson equation

$$-\nabla\cdot\varepsilon(\phi)\nabla\Phi = 4\pi e(Z_1n_1 + Z_2n_2). \tag{2.2}$$

The dielectric constant $\varepsilon(\phi)$ can depend on the composition ϕ. In our previous work the linear composition dependence

$$\varepsilon(\phi) = \varepsilon_0 + \varepsilon_1\phi \tag{2.3}$$

has been assumed, where ε_0 is the dielectric constant of the less-polar component and $\varepsilon_0 + \varepsilon_1$ is that of the water-like component. In such cases $\varepsilon_0 > 0$ and $\varepsilon_1 > 0$. This linear form approximately holds in some polar binary mixtures [20]. The last term in (2.1) consists of the entropic part and the solvation contribution of the ions, where the parameters g_j represent the solvation strength. The choice of the volume v_0 is arbitrary and is taken to be the solvent molecular volume (see (5.1) below). In this work we neglect the image interaction arising from inhomogeneous dielectric constant or from nonvanishing ε_1 in our theory [5, 6, 21]. The interfacial ion distribution is then produced by the preferential solvation among the ions and the mixture solvent. The image interaction is weakened with increasing the salt density and/or approaching the critical point.

With (2.1) we may calculate the chemical potentials $h = \delta F/\delta\phi$ and $\mu_j = \delta F/\delta n_j$. They are written as

$$\frac{h}{T} = \frac{f_0'}{T} - C\nabla^2\phi - \frac{\varepsilon_1\boldsymbol{E}^2}{8\pi T} - \sum_j g_j n_j, \tag{2.4}$$

$$\frac{\mu_j}{T} = \ln(n_j v_0) - g_j\phi + \frac{1}{T}Z_j e\Phi, \tag{2.5}$$

where $f_0' = \partial f_0(\phi)/\partial\phi$ and $\varepsilon_1 = \partial\varepsilon/\partial\phi$. If the system is in equilibrium, h, μ_1, and μ_2 are homogeneous constants. When the system undergoes a macroscopic phase separation with a planar interface separating polar and less-polar regions, we may calculate the interface profiles of the composition and the ions [6]. In equilibrium the composition difference $\Delta\phi$ and the potential difference $\Delta\Phi$ satisfy

$$e\Delta\Phi = T(g_1 - g_2)\Delta\phi/(Z_1 + |Z_2|), \tag{2.6}$$

from the charge neutrality in the bulk regions. The $\Delta\Phi$ is called the Galvani potential difference in electrochemistry [22, 23].

The solvation free energy may be written as $f_{\rm sol} = \sum_j \mu^j_{\rm sol}(\phi)n_j$, where $\mu^j_{\rm sol}(\phi)$ is the solvation chemical potential of the ion species j. It is assumed to depend on ϕ as

$$\mu^j_{\rm sol}(\phi) = \mu^j_{\rm sol}(0) - Tg_j\phi. \tag{2.7}$$

Here the first term in the right-hand side gives a contribution linear in n_j in $f_{\rm sol}$ and is not written in f in (2.1), while the second term yields the solvation coupling terms in f between the ions and the composition. We remark on the magnitude of g_j. In aqueous mixtures, it is positive for hydrophilic ions and negative for hydrophobic ions. In two-phase coexistence, the difference of the solvation chemical potential between the two phases is given by $\Delta\mu^j_{\rm sol} = Tg_j\Delta\phi$, which is identical to the standard Gibbs transfer free energy (per particle) in electrochemistry [22, 23]. Data of $\Delta\mu^j_{\rm sol}$ are available for water-nitrobenzene at room temperatures in strong segregation (where $\Delta\phi \cong 1$). For example, $\Delta\mu^j_{\rm sol}/T = g_j\Delta\phi = 13.6$ for Na^+, 15.3 for Li^+, 26.9 for Ca^{2+}, 11.3 for Br^-, and 7.46 for I^- as examples of hydrophilic ions, while it is -14.4 for BPh_4^- (tetraphenylborate) as an example of hydrophobic ions. The anion BPh_4^- consists of four phenyl rings bonded to an ionized boron, acquiring strong hydrophobicity. Note that Sadakane *et al* [16, 17] used $NaBPh_4$. Thus the preferential solvation effect can be very strong. However, it has mostly been neglected in theories of electrolytes and soft matters, though it strongly influences phase transitions in such systems.

When phase separation occurs macroscopically, a liquid–liquid interface appears. If the space dependence is along the z

axis, the surface tension is expressed as [10]

$$\gamma = 2\int \mathrm{d}z\,(f_{\rm g} - f_{\rm el}), \tag{2.8}$$

where $f_{\rm g} = C|\nabla\phi|^2/2$ is the gradient free energy density and $f_{\rm el} = \varepsilon \boldsymbol{E}^2/8\pi$ is the electrostatic free energy density. Up to linear order in the ion densities, we may also derive the expression,

$$\gamma \cong \gamma_0 - T\Gamma + \gamma_{\rm el}, \tag{2.9}$$

where γ_0 is the surface tension without ions, Γ is the surface adsorption of ions, and $\gamma_{\rm el}$ is the electrostatic contribution given by $\gamma_{\rm el} = -\int \mathrm{d}z\, f_{\rm el} < 0$. For antagonistic salts with large $|g_i|$, $|\gamma_{\rm el}|$ is much amplified due to the electric double layer at the interface.

2.2. Structure factor in one-phase states

In our previous papers [5, 6], we examined the structure factor $S(q) = \langle|\phi_{\boldsymbol{q}}|^2\rangle$ of the composition fluctuations with wavenumber $q = |\boldsymbol{q}|$ in one-phase states with salt, where $\phi_{\boldsymbol{q}}$ is the Fourier component of the composition deviation $\delta\phi(\boldsymbol{r}) = \phi(\boldsymbol{r}) - \langle\phi\rangle$ with wavevector $\boldsymbol{q}$. Hereafter $\langle\cdots\rangle$ denotes the thermal average. We readily obtain $S(q)$ if the fluctuation contributions to F are calculated in the bilinear order. The resultant free energy part is written as δF. The thermal fluctuations obey the Gaussian distribution $\propto \mathrm{e}^{-\delta F/T}$ in equilibrium in the mean-field theory. Hereafter we consider the monovalent case $Z_1 = -Z_2 = 1$, where the average ion densities are written as $\langle n_1\rangle = \langle n_2\rangle = n_e$.

From (2.1) some calculations give

$$\delta F = \frac{T}{2}\sum_{\boldsymbol{q}}\left[(\bar{r} + Cq^2)|\phi_{\boldsymbol{q}}|^2 + \frac{4\pi\ell_{\rm B}}{q^2}|\rho_{\boldsymbol{q}}|^2\right] + T\sum_{\boldsymbol{q}}\sum_j\left[\frac{1}{2n_e}|n_{j\boldsymbol{q}}|^2 - g_j n_{j\boldsymbol{q}}\phi^*_{\boldsymbol{q}}\right], \tag{2.10}$$

where $n_{j\boldsymbol{q}}$ and $\rho_{\boldsymbol{q}}$ are the Fourier components of $n_j(\boldsymbol{r})$ and $\rho(\boldsymbol{r}) \equiv n_1(\boldsymbol{r}) - n_2(\boldsymbol{r})$, respectively, and $\ell_{\rm B} = e^2/\varepsilon T$ is the Bjerrum length. We define

$$\bar{r} = \partial^2 f_0(\phi)/\partial\phi^2. \tag{2.11}$$

The average composition $\langle\phi\rangle$ is simply written as ϕ. Here we may treat ε as a constant when we treat the small thermal fluctuations. By minimizing δF with respect to $n_{j\boldsymbol{q}}$ at fixed $\phi_{\boldsymbol{q}}$, we obtain $\delta F/T = \sum_{\boldsymbol{q}}|\phi_{\boldsymbol{q}}|^2/2S(q)$ with

$$\frac{1}{S(q)} = \bar{r} - (g_1+g_2)^2\frac{n_e}{2} + Cq^2\left[1 - \frac{\gamma_p^2\kappa^2}{\kappa^2+q^2}\right], \tag{2.12}$$

where $\kappa = (8\pi\ell_{\rm B}n_e)^{1/2}$ is the Debye wavenumber and the parameter

$$\gamma_p = (16\pi C\ell_{\rm B})^{-1/2}|g_1 - g_2| \tag{2.13}$$

represents asymmetry of the solvation of the two ion species. The structure factor thus obtained is analogous to that for weakly charged polyelectrolytes [10, 24, 25].

The second term in the right-hand side of (2.12) gives rise to a shift of the spinodal curve [12]. For example, if the cations and anions are hydrophilic and $g_1 \sim g_2 \sim 15$, the shift term is of order $-500n_e$ and its magnitude can be appreciable even for $v_0 n_e \ll 1$. On the other hand, γ_p can be increased for antagonistic salts composed of hydrophilic and hydrophobic ions [5, 6, 16, 17]. From the last term in (2.12) a Lifshitz point appears at $\gamma_p = 1$. For $\gamma_p > 1$, $S(q)$ exhibits a peak at an intermediate wavenumber q_m. Since the derivative of the right-hand side of (2.12) with respect to q^2 vanishes at $q = q_m$, we find

$$q_m = (\gamma_p - 1)^{1/2}\kappa. \tag{2.14}$$

The peak height is given by $S(q_m) = 1/(\bar{r} - r_m)$, where

$$r_m = (g_1+g_2)^2\frac{n_e}{2} + C(\gamma_p - 1)^2\kappa^2. \tag{2.15}$$

For $\bar{r} < r_m$, mesophase formation takes place, as will be studied in section 4.

3. Dynamics

3.1. Dynamic equations for composition, ions, and velocity

We present the dynamic equations for ϕ, n_1, n_2, and the velocity field $\boldsymbol{v}$ [26]. The fluid is assumed to be incompressible and isothermal. That is, we require

$$\nabla\cdot\boldsymbol{v} = 0 \tag{3.1}$$

and treat the mass density ρ_0 and the temperature T as constants. Then ϕ and n_j obey

$$\frac{\partial\phi}{\partial t} + \nabla\cdot(\phi\boldsymbol{v}) = L_0\nabla^2\frac{h}{T}, \tag{3.2}$$

$$\frac{\partial n_j}{\partial t} + \nabla\cdot(n_j\boldsymbol{v}) = D_j\nabla\cdot n_j\nabla\frac{\mu_j}{T} = D_j\nabla\cdot\left[\nabla n_j - \frac{Z_j e}{T}n_j\boldsymbol{E} - g_j n_j\nabla\phi\right], \tag{3.3}$$

where h and μ_j are given in (2.4) and (2.5), L_0 is the kinetic coefficient (with L_0/v_0 representing a diffusion constant), and D_1 and D_2 are the ion diffusion constants in the solvent. The momentum equation is expressed as

$$\rho_0\frac{\partial\boldsymbol{v}}{\partial t} = -\nabla p_1 - \nabla\cdot\overleftrightarrow{\boldsymbol{\Pi}} + \eta_0\nabla^2\boldsymbol{v}, \tag{3.4}$$

The first term on the right-hand side ensures the incompressibility condition (3.1) and p_1 satisfies

$$\nabla^2 p_1 = -\sum_{\alpha\beta}\nabla_\alpha\nabla_\beta\Pi_{\alpha\beta}, \tag{3.5}$$

where $\nabla_\alpha = \partial/\partial x_\alpha$ with $x_\alpha = x, y, z$. We introduce the reversible stress tensor $\overleftrightarrow{\boldsymbol{\Pi}} = \{\Pi_{\alpha\beta}\}$ $(\alpha, \beta = x, y, z)$ in the form,

$$\Pi_{\alpha\beta} = TC\nabla_\alpha\phi\nabla_\beta\phi - \frac{\varepsilon}{4\pi}E_\alpha E_\beta \tag{3.6}$$

where the first term is well known in critical dynamics [26] and the second term is a part of the Maxwell stress tensor (with its diagonal part being included in p_1) [27].

We determine $\overleftrightarrow{\Pi}$ from the relation,

$$\nabla \cdot \overleftrightarrow{\Pi} = \phi \nabla h + \sum_j n_j \nabla \mu_j. \tag{3.7}$$

If the above relation holds, the total free energy $F_{\rm T} = \int {\rm d}\boldsymbol{r}\,[f + \rho_0 \boldsymbol{v}^2/2]$ including the fluid kinetic energy changes in time as

$$\frac{\rm d}{{\rm d}t} F_{\rm T} = -\int {\rm d}\boldsymbol{r}\,[\dot{\epsilon}_\phi + \dot{\epsilon}_{\rm vis} + \dot{\epsilon}_{\rm ion}], \tag{3.8}$$

where the terms in the brackets are the heat production rates in the bulk given by

$$\dot{\epsilon}_\phi = L_0 |\nabla h|^2, \qquad \dot{\epsilon}_{\rm vis} = \eta_0 \sum_{\alpha\beta} |\nabla_\alpha v_\beta|^2,$$
$$\dot{\epsilon}_{\rm ion} = \sum_j D_j n_j |\nabla \mu_j|^2 / T. \tag{3.9}$$

The surface terms are omitted in (3.8). Owing to ${\rm d}F_{\rm T}/{\rm d}t \leqslant 0$, the system tends to equilibrium if there is no externally applied flow.

In our dynamic equations we neglect the random source terms [26], which are related to the transport coefficients L_0, D_j, and η_0 via the fluctuation–dissipation relations. They are needed to describe the dynamics of the thermal fluctuations and to calculate the time-correlation functions.

3.2. Stokes approximation

Without macroscopic flow, the viscous motion of $\boldsymbol{v}$ is much faster than the diffusive motions of ϕ and n_j. Here L_0/v_0, D_1, and D_2 are estimated by the Stokes formula ($D_j \sim T/6\pi\eta_0 a_j$ with a_j being the molecular size), so they are much smaller than the kinematic viscosity η_0/ρ_0. Then we may well neglect the acceleration of the velocity in (3.4) to obtain [26]

$$v_\alpha(\boldsymbol{r}) = \int {\rm d}\boldsymbol{r}' \sum_\beta \mathcal{T}_{\alpha\beta}(\boldsymbol{r} - \boldsymbol{r}') X_\beta(\boldsymbol{r}') \tag{3.10}$$

where $X_\alpha(\boldsymbol{r}) = -\sum_\beta \nabla_\beta \Pi_{\alpha\beta}(\boldsymbol{r})$ is the force density acting on the fluid and $\mathcal{T}_{\alpha\beta}(\boldsymbol{r})$ is the Oseen tensor. This Stokes approximation has been used in numerical analysis of spinodal decomposition in the literature [28]. The free energy $F = \int {\rm d}\boldsymbol{r}\, f$ changes in time as ${\rm d}F/{\rm d}t = -\int {\rm d}\boldsymbol{r}\,[\dot{\epsilon}_\phi + \dot{\epsilon}_{\rm vis} + \dot{\epsilon}_{\rm ion}] \leqslant 0$ as in (3.8), where $\dot{\epsilon}_{\rm vis}$ is replaced by

$$\dot{\epsilon}_{\rm vis} = \sum_\alpha X_\alpha v_\alpha. \tag{3.11}$$

Here $\int {\rm d}\boldsymbol{r}\, \dot{\epsilon}_{\rm vis} \geqslant 0$ from the expression (3.10).

3.3. Ionic local equilibrium

The composition evolution can be much slower than the ionic motions particularly near the critical point. In such cases, the ion distributions are expressed in terms of ϕ and Φ as

$$n_j = n_j^0 \exp(g_j \phi - Z_j e \Phi / T), \tag{3.12}$$

where the coefficient n_j^0 is determined from the conservation of the ions $\int {\rm d}\boldsymbol{r}\, n_j(\boldsymbol{r}, t) = $ const. In numerical analysis this approximation is convenient to examine the mesophase formation for large g_j.

4. Relaxation of the thermal composition fluctuations

4.1. Time-correlation function

In this section, we calculate the time-correlation function of the Fourier components of the composition fluctuations,

$$G(q, t) = \langle \phi_q(t) \phi_q(0)^* \rangle, \tag{4.1}$$

in one-phase states. This function can be measured by dynamic scattering. It is of interest how it relaxes on approaching the spinodal point and how it is influenced by the ion diffusion. The thermal hydrodynamic fluctuations are governed by the linearized hydrodynamic equations of (3.2) and (3.3) with random source terms added. That is, they obey linear Langevin equations [26]. In this section, without explicit introduction of the noise terms, we will calculate the time-correlation functions of the form $\langle \mathcal{A}_q(t) \phi_q(0)^* \rangle$ with $t > 0$, where $\mathcal{A} = \phi$, n_1, and n_2. We also assume that the cations and the anions have the same diffusion constant or $D_2 = D_1$, which much simplifies the calculation.

From (3.3) $G(q, t)$ obeys the linear equation,

$$\left[\frac{\partial}{\partial t} + \Gamma_0(q)\right] G = L_0 q^2 \Big[g_1 G_1 + g_2 G_2\Big], \tag{4.2}$$

where $G(q, t)$ is written as G and $\Gamma_0(q)$ is the decay rate without ions,

$$\Gamma_0(q) = L_0 q^2 (\bar{r} + C q^2). \tag{4.3}$$

Here we write $G_1 \equiv \langle n_{1q}(t) \phi_q(0)^* \rangle$ and $G_2 \equiv \langle n_{2q}(t) \phi_q(0)^* \rangle$, where n_{1q} and n_{2q} are the Fourier components of n_1 and n_2. The equations for the combinations $G_1 \pm G_2$ read

$$\left[\frac{\partial}{\partial t} + D_1 q^2\right](G_1 + G_2) = n_e (g_1 + g_2) D_1 q^2 G, \tag{4.4}$$

$$\left[\frac{\partial}{\partial t} + D_1 (q^2 + \kappa^2)\right](G_1 - G_2) = n_e (g_1 - g_2) D_1 q^2 G. \tag{4.5}$$

Use has been made of the fact that the Fourier component of the electric potential is $\Phi_q = 4\pi e (n_{1q} - n_{2q})/\varepsilon q^2$ from the Poisson equation (2.2), where the dielectric constant ε may be treated as a constant. The convective terms in (3.2) and (3.3) vanish in the linear order without velocity gradient.

It is convenient to calculate the Laplace transformation

$$\hat{G}(q, \Omega) = \int_0^\infty {\rm d}t\, {\rm e}^{-\Omega t} G(q, t). \tag{4.6}$$

The Fourier transformation $I(q, \omega) = \int_{-\infty}^{\infty} {\rm d}t\, {\rm e}^{-{\rm i}\omega t} G(q, t)$ is related to $\hat{G}(q, \Omega)$ by

$$I(q, \omega) = 2\,{\rm Re}[\hat{G}(q, {\rm i}\omega)], \tag{4.7}$$

where ${\rm Re}[\cdots]$ denotes taking the real part. Some calculations give the following expression,

$$\hat{G}(q, \Omega) = S(q) \left[\Omega + \frac{L_0 q^2 / S(q)}{1 + Z(q, \Omega)}\right]^{-1}. \tag{4.8}$$

The ionic correction $Z(q,\Omega)(\propto n_e)$ depends on q and Ω as

$$Z(q,\Omega)=\frac{1}{2}n_eL_0q^2\Big[\frac{(g_1+g_2)^2}{\Omega+D_1q^2} + \frac{(g_1-g_2)^2q^2}{[\Omega+D_1(q^2+\kappa^2)](q^2+\kappa^2)}\Big]. \tag{4.9}$$

In deriving (4.8) and (4.9) use has also been made of the static relations,

$$\begin{aligned}\langle(n_{1q}+n_{2q})\phi_q^*\rangle &= n_e(g_1+g_2)S(q),\\ (1+\kappa^2/q^2)\langle(n_{1q}-n_{2q})\phi_q^*\rangle &= n_e(g_1-g_2)S(q),\end{aligned} \tag{4.10}$$

which follow from (2.10). These equal-time-correlation functions appear in the Laplace transformation of $S(q,t)$ in the presence of the random source terms. The presence of $Z(q,\Omega)$ in (4.8) makes the relaxation of $G(q,t)$ complicated.

4.2. Relaxation near the spinodal point

We obtain the exponential relaxation,

$$G(q,t)\cong S(q)\mathrm{e}^{-\Gamma(q)t}, \tag{4.11}$$

near the spinodal point. Here the decay rate $\Gamma(q)$ is assumed to be much smaller than D_1q^2. Then we may set $\Omega=0$ in $Z(q,\Omega)$ to find

$$\Gamma(q)\cong\frac{L_0q^2/S(q)}{1+n_eB(q)}, \tag{4.12}$$

where $B(q)=Z(q,0)/n_e$ is written as

$$B(q)=\frac{L_0}{D_1}\Big[\frac{(g_1+g_2)^2}{2}+\frac{(g_1-g_2)^2q^4}{2(q^2+\kappa^2)^2}\Big]. \tag{4.13}$$

If $|g_1|$ and $|g_2|$ are very large, the ionic correction $n_eB(q)$ can be noticeable even for $v_0n_e\ll1$. For $\gamma_p>1$, $\Gamma(q)$ tends to zero first at $q=q_m$ on approaching the spinodal point.

4.3. Long wavelength limit

In dynamic light scattering experiments, we should consider the long wavelength limit, where we set $q\ll\kappa$, $\Gamma_0(q)\cong D_\phi q^2$, and $Z(q,\Omega)\cong\alpha D_1q^2/(\Omega+D_1q^2)$ with

$$D_\phi=L_0\bar{r}, \tag{4.14}$$

$$\alpha=L_0(g_1+g_2)^2n_e/2D_1. \tag{4.15}$$

Here $D_\phi=\lim_{q\to0}\Gamma(q)/q^2$ is the diffusion constant of the composition in the long wavelength limit without ions. The dimensionless parameter α is proportional to n_e and increases steeply with increasing n_e for $g_1+g_2\gg1$. In dynamic light scattering without ions, D_ϕ tends to zero near the critical point (being given by the Kawasaki formula $T/6\pi\eta_0\xi$ with ξ being the correlation length) [26]. In this limit we obtain

$$\begin{aligned}\frac{\hat{G}(q,\Omega)}{S(q)}&=\frac{\Omega+(1+\alpha)D_1q^2}{\Omega^2+\mathcal{D}q^2\Omega+D_1D_\phi q^4}\\ &=\frac{\beta}{\Omega+D_-q^2}+\frac{1-\beta}{\Omega+D_+q^2},\end{aligned} \tag{4.16}$$

where $\mathcal{D}=(1+\alpha)D_1+D_\phi$ in the first line. The two new diffusion constants D_- and D_+ in the second line are expressed as

$$D_\pm=\frac{\mathcal{D}}{2}\pm\frac{1}{2}\sqrt{\mathcal{D}^2-4D_\phi D_1}. \tag{4.17}$$

The partition coefficient β is of the form

$$\beta=\frac{1}{2}+\frac{(1+\alpha)D_1-D_\phi}{2(D_+-D_-)}. \tag{4.18}$$

The inverse Laplace transformation of the second line of (4.15) yields the time-correlation function exhibiting a double-exponential decay,

$$\frac{G(q,t)}{S(q)}=\beta\mathrm{e}^{-D_-q^2t}+(1-\beta)\mathrm{e}^{-D_+q^2t}. \tag{4.19}$$

(i) For very small ion concentrations there can be the situation where $\alpha\ll1$ and $D_1\alpha\ll D_\phi<D_1$. In this case we have $D_-\cong D_\phi$ and $D_+\cong D_1$ with $\beta=1-\alpha D_\phi/(D_1-D_\phi)^2+\cdots$. (ii) We may suppose the case $D_s\ll D_1\alpha$. In this case we have $D_-\cong D_\phi/(1+\alpha)$, $D_+\cong D_1(1+\alpha)$, with $\beta=1-[(2\alpha-1)/2(1+\alpha)^2]D_\phi/D_1+\cdots$.

5. Simulations at the critical composition

We numerically examine phase ordering with a strongly antagonistic salt at the critical composition $\langle\phi\rangle=1/2$. The spatial dimensionality d has been equal to three so far. However, we here present preliminary simulation results in two dimensions.

5.1. Numerical method

In our simulation, we choose the chemical free energy density f_0 in (2.1) in the Bragg–Williams form,

$$\frac{v_0}{T}f_0=\phi\ln\phi+(1-\phi)\ln(1-\phi)+\chi\phi(1-\phi), \tag{5.1}$$

where $v_0=a^d$ is the solvent molecular volume and χ is the interaction parameter dependent on T. The parameter $\bar{r}$ in (2.9) is given by $\bar{r}=[1/\phi(1-\phi)-2\chi]/v_0$. Space and time will be measured in units of a and

$$t_0=v_0a^2/L_0, \tag{5.2}$$

where L_0 is the kinetic coefficient in (3.2). Integration of the dynamic equations is performed on a 256×256 square lattice, so the system is in the region $0<x,y<256a$. Supposing the monovalent case, we set

$$\begin{aligned}&v_0C=a^2, \qquad g_1=-g_2=15,\\ &\varepsilon_1=0, \qquad \ell_B=3a, \qquad \frac{\eta_0}{T}=\frac{0.16a^4}{L_0}.\end{aligned} \tag{5.3}$$

Then we obtain $\gamma_p\cong2.44$ from (2.11) and mesophases are realized with increasing χ. These values of g_1 and g_2 are realistic in view of the data of the Gibbs transfer free energy, as discussed below (2.7). The correlation length is defined by $\xi=[Cv_0/|4-2\chi|]^{1/2}$, which is equal to a for $\chi=2.5$.

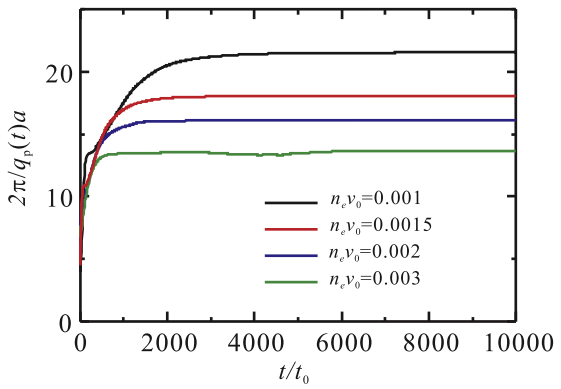

Figure 1. Characteristic domain size $2\pi/q_m(t)a$ versus time at the solvent criticality for $v_0 n_e = 0.001, 0.0015, 0.002$, and 0.003. The saturated value of $q_p(t)$ nearly coincides with q_m in (2.14).

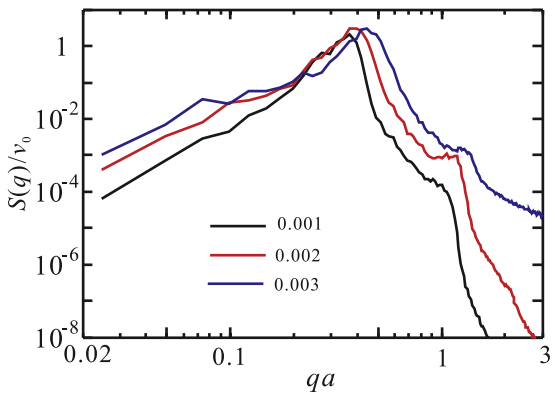

Figure 2. Steady-state structure factor $S(q)$ of the composition for $v_0 n_e = 0.001, 0.002$, and 0.003, where the solvent is at the criticality ($\chi = 2$ and $\langle\phi\rangle = 1/2$).

The velocity field $\boldsymbol{v}$ is determined by the Stokes approximation (3.10) and the ion densities n_1 and n_2 by the Poisson–Boltzmann expressions (3.12) (the latter being justified in the limit $D_j \to \infty$). In the dynamic equation (3.2) for ϕ we put a random source term to calculate the structure factor,

$$\frac{\partial\phi}{\partial t} + \nabla\cdot(\phi\boldsymbol{v}) = L_0\nabla^2\frac{h}{T} - \nabla\cdot\boldsymbol{j}_{\rm R}, \tag{5.4}$$

Here $\boldsymbol{j}_{\rm R}$ is the random diffusion flux characterized by

$$\langle j_{{\rm R}\alpha}(\boldsymbol{r},t)\, j_{{\rm R}\beta}(\boldsymbol{r}',t')\rangle = 2\tilde{L}\delta_{\alpha\beta}\delta(\boldsymbol{r}-\boldsymbol{r}')\delta(t-t') \tag{5.5}$$

where $\alpha, \beta = x, y$. The noise strength $\tilde{L}$ should be equal to the kinetic coefficient L_0 to ensure the equilibrium distribution ($\propto {\rm e}^{-F/T}$). In this paper, however, we set $\tilde{L} = 10^{-8}L_0$ to detect the composition patterns unambiguously. In one-phase states, ϕ remains nonvanishing due to $\boldsymbol{j}_{\rm R}$, yielding a structure factor proportional to the mean-field structure factor $S(q)$ in (2.12), where the proportionality constant is $\tilde{L}/L_0 = 10^{-8}$ (not shown here). In two-phase states, $\boldsymbol{j}_{\rm R}$ serves to trigger phase ordering, yielding a structure factor composed of the domain contribution. The same structure factor follows even if we set $\boldsymbol{j}_{\rm R} = \boldsymbol{0}$ in the course of domain growth. It is worth noting that the random source terms are mostly neglected in the literature of phase ordering dynamics [26].

In our simulations we start with the initial condition $\phi(\boldsymbol{r}, 0) = 1/2$ at $t = 0$. Small disturbances of ϕ are subsequently produced by the small random flux $\boldsymbol{j}_{\rm R}$ in (5.4), which grow into patterns in two-phase states. For $g_1 = -g_2$ and $\langle\phi\rangle = 0.5$, use of (2.15) yields the linear instability criterion,

$$2 - \chi < \tfrac{1}{2}Ca^2(\gamma_p - 1)^2\kappa^2, \tag{5.6}$$

where the right-hand side is $78v_0n_e$ from (5.3). Hereafter the Debye wavenumber is $\kappa = 8.7n_e^{1/2}$ with $n_e = \langle n_1\rangle = \langle n_2\rangle$ being the average ion density.

5.2. Mesophase formation in shallow quenching

Here we study the phase ordering at the solvent criticality $\chi = 2$ and $\langle\phi\rangle = 1/2$, where instability occurs for $n_e > 0$. In figure 1, we show the time evolution of a normalized characteristic domain size $2\pi/aq_p(t)$ for various n_e. In terms of the time-dependent structure factor $S(q,t) = \langle|\phi_{\boldsymbol{q}}(t)|^2\rangle$ we define

$$q_p(t) = \sum_{\boldsymbol{q}} q\, S(q,t) \Big/ \sum_{\boldsymbol{q}} S(q,t). \tag{5.7}$$

In this shallow quenching, the random source terms in the dynamic equations can greatly change the structure factor if their magnitudes are on the order of the thermal noise.

In figure 1, $q_p(t)$ tends to a constant expressed as $9.22n_e^{1/2}$ at long times. It nearly coincides with $q_m = (\gamma_p - 1)^{1/2}\kappa = 10.4n_e^{1/2}$ in (2.14). In figure 2, the steady-state structure factor $S(q)$ is given for three ion densities, where all the curves arise from the domain structure and are not affected by the small noise term in (5.4). Our $S(q)$ exhibits a sharp peak at $q = q_m$ and a second peak at $q = 3q_m$. The peak height at $q = q_m$ is a constant of order unity nearly independent of n_e. This can be explained as follows. It is known that a domain structure gives the structure factor of the form $S(q) \cong (\Delta\phi)^2\ell^d S^*(q\ell)$, where $\Delta\phi$ is the composition difference between the two phases, ℓ is the domain size, and $S^*(x)$ is a scaling function. In our two-dimensional case, we have $\Delta\phi \propto n_e^{1/2}$ and $\ell \sim 2\pi/q_m \propto n_e^{-1/2}$, so $S(q) \sim S^*(q\ell)$.

In figure 3, we display $\phi(\boldsymbol{r},t)$ and $n_1(\boldsymbol{r},t)$ at $t = 3000t_0$ for $v_0n_e = 0.0005$ (left) and 0.0025 (right). In figure 4, we present cross sections of ϕ, n_1, n_2 in the upper panel and those of the gradient free energy $f_{\rm g} = TC|\nabla\phi|^2/2$ and the electrostatic energy $f_{\rm e} = \varepsilon\boldsymbol{E}^2/8\pi$, and their difference in the lower panel. These quantities vary mildly without sharp interfaces as functions of x at fixed $y = 64a$. We notice that the difference $f_{\rm g} - f_{\rm e}$ is small. In figure 5, their space averages, $\langle f_{\rm g}\rangle = \int {\rm d}\boldsymbol{r}\, f_{\rm g}/V$ and $\langle f_{\rm e}\rangle = \int {\rm d}\boldsymbol{r}\, f_{\rm e}/V$, are demonstrated to be nearly the same at long times, where V is the system volume.

We argue why $\langle f_{\rm g}\rangle \cong \langle f_{\rm e}\rangle$ holds in steady states in weak segregation. If the ion density is small at shallow quenching, the composition is weakly segregated and is composed of the Fourier components with $q = |\boldsymbol{q}| \cong q_m$. As in the weak segregation case of block copolymers [29], the deviation $\delta\phi = \phi - \langle\phi\rangle$ is expressed as

$$\delta\phi = \sum_{\boldsymbol{q}} A_{\boldsymbol{q}}\, {\rm e}^{{\rm i}\boldsymbol{q}\cdot\boldsymbol{r}}, \tag{5.8}$$

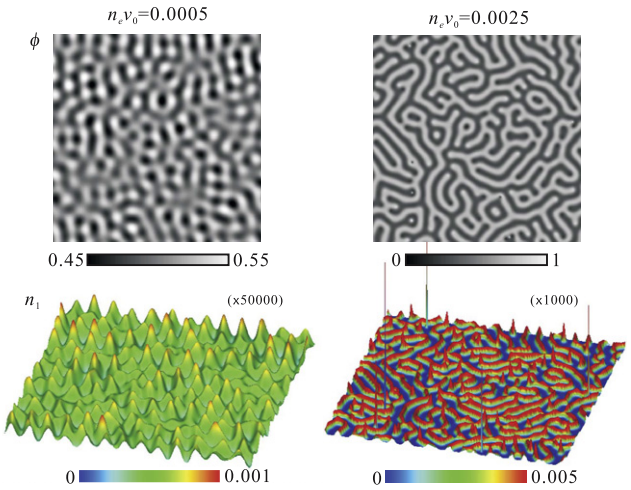

Figure 3. Patterns of $\phi(\boldsymbol{r}, t)$ (top) and $n_1(\boldsymbol{r}, t)$ (bottom) at $t = 3000t_0$ for $n_e v_0 = 0.0005$ (left) and 0.0025 (right) at the solvent criticality.

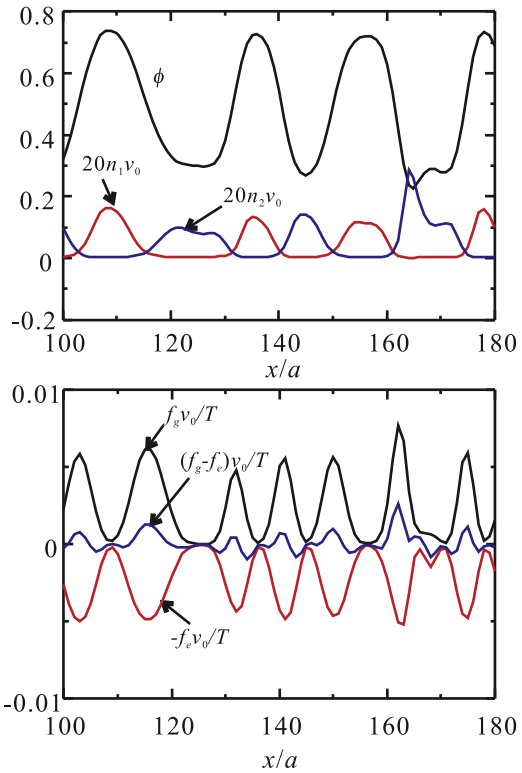

Figure 4. Cross sections of ϕ, $v_0 n_1$, and $v_0 n_2$ (top) and those of $f_g v_0/T$, $-f_e v_0/T$, and $(f_g - f_e)v_0/T$ (bottom) for $n_e v_0 = 0.0025$ in the region $100 < x < 180$ at $y = 64$, where the solvent is at the criticality. Use is made of the data producing the right images in figure 3.

where the coefficients A_q are sharply peaked at $q = q_m$. With this form, the space average of f_g is written as

$$\frac{\langle f_g\rangle}{T} = \frac{1}{2V}\sum_q q^2|A_q|^2 \cong \tfrac{1}{2}Cq_m^2\langle\delta\phi^2\rangle, \tag{5.9}$$

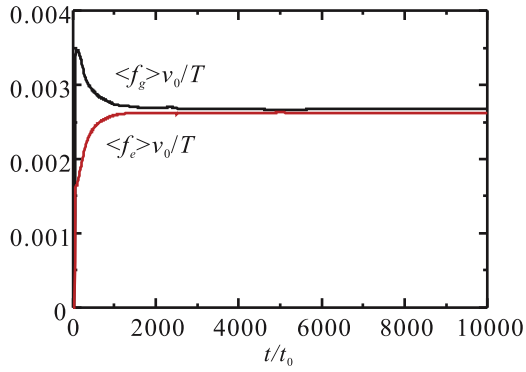

Figure 5. Space averages of $f_g v_0/T = v_0 C|\nabla\phi|^2/2$ and $f_e v_0/T = v_0\varepsilon|\nabla\Phi|^2/8\pi T$ versus time t for $n_e v_0 = 0.0025$, where the solvent is at the criticality.

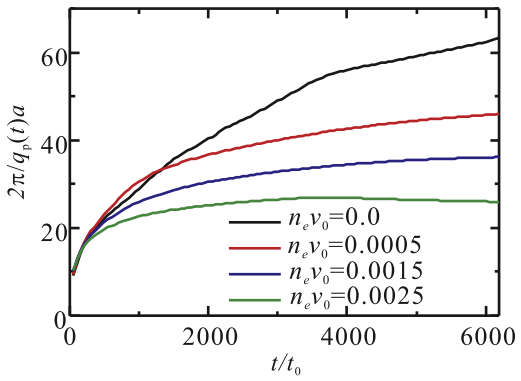

Figure 6. Characteristic domain size $2\pi/q_m(t)a$ versus time in deep quenching with $\chi = 2.5$ and $\langle\phi\rangle = 1/2$ for $v_0 n_e = 0$, 0.0005, 0.0015, and 0.0025.

where $\langle\delta\phi^2\rangle = \sum_q |A_q|^2/V$. Linearizing (2.2) and (3.12) with respect to $\delta\phi$ in the monovalent case, we obtain the electric potential [10],

$$\Phi = \frac{T}{2e}\sum_q \frac{(g_1 - g_2)\kappa^2}{q^2 + \kappa^2} A_q\, \mathrm{e}^{\mathrm{i}\boldsymbol{q}\cdot\boldsymbol{r}}. \tag{5.10}$$

From (2.13) the average electrostatic energy is written as

$$\frac{\langle f_e\rangle}{T} = \frac{1}{2V}\sum_q \frac{C\gamma_p^2\kappa^4 q^2}{(q^2+\kappa^2)^2}|A_q|^2 \cong \frac{C\gamma_p^2\kappa^4 q_m^2}{2(q_m^2+\kappa^2)^2}\langle\delta\phi^2\rangle. \tag{5.11}$$

From $q_m = (\gamma_p - 1)^{1/2}\kappa$ in (2.14), we find $\langle f_g\rangle \cong \langle f_e\rangle$.

5.3. Mesophase formation in deep quenching

Next we examine the case of deep quenching by setting $\chi = 2.5$ with $\langle\phi\rangle = 0.5$, where the interface thickness is $\xi = a$. In figure 6, we show the time evolution of the characteristic domain size $2\pi/q_p(t)$, where $q_p(t)$ is defined by (5.7). For $v_0 n_e = 0.0025$ the domain size approaches a constant, while for $v_0 n_e = 0.0015$ and 0.0005 its growth still continues in the simulation but is extremely slow at the end of the simulation

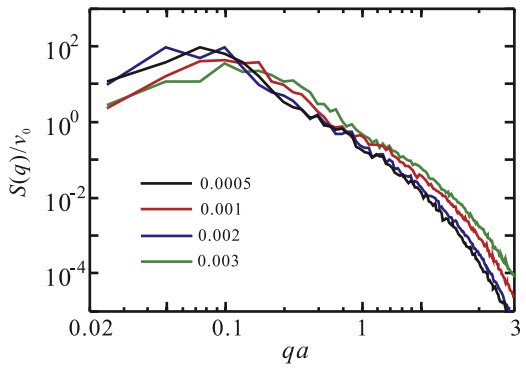

Figure 7. Structure factor $S(q)$ in deep quenching with $\chi = 2.5$ and $\langle\phi\rangle = 1/2$ for $v_0 n_e = 0, 0.0005, 0.001, 0.0015$, and 0.0025. The numbers in the figure denote $n_e v_0$.

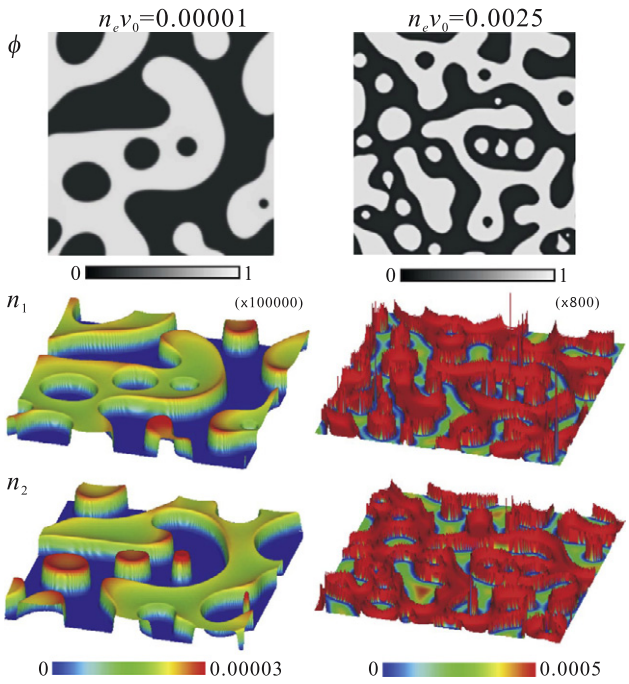

Figure 8. Patterns of $\phi(\boldsymbol{r})$ (top), $n_1(\boldsymbol{r})$ (middle), and $n_2(\boldsymbol{r})$ (bottom) in deep quenching at $t = 3000t_0$ for $n_e v_0 = 0.000\,01$ (left) and 0.0025 (right), where $\chi = 2.5$ and $\langle\phi\rangle = 1/2$.

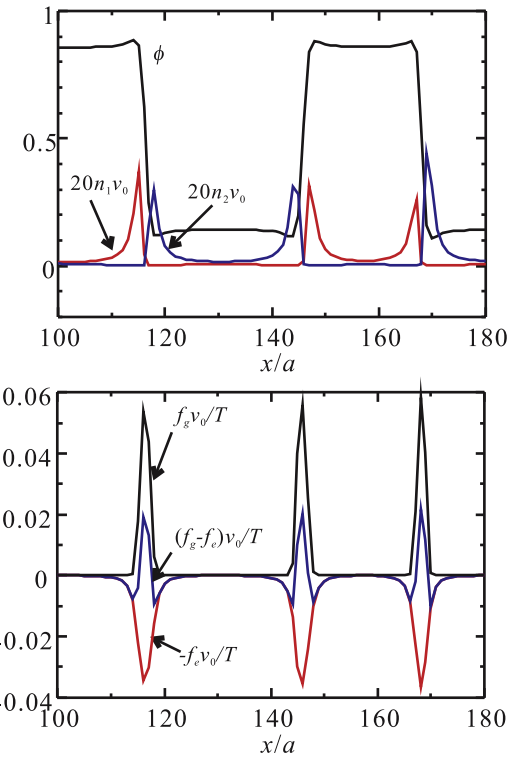

Figure 9. Cross sections of ϕ, $v_0 n_1$, and $v_0 n_2$ (upper plate) and those of $f_g v_0/T$, $-f_e v_0/T$, and $(f_g - f_e)v_0/T$ (lower plate) for $n_e v_0 = 0.0025$ in the region $100 < x < 180$ at $y = 64$, where $\chi = 2.5$ and $\langle\phi\rangle = 1/2$. Use is made of the data producing the right images in figure 8.

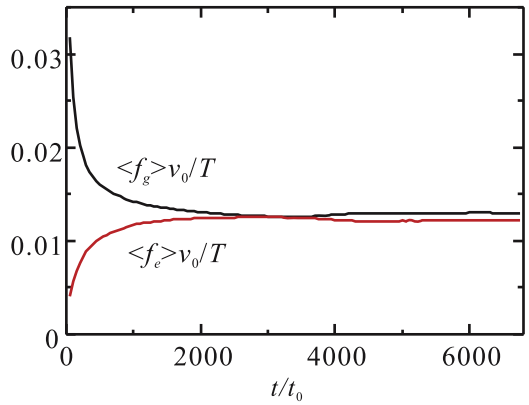

Figure 10. Space averages of $f_g v_0/T$ and $f_e v_0/T$ versus time t for $n_e v_0 = 0.0025$, where $\chi = 2.5$ and $\langle\phi\rangle = 1/2$.

$(t/t_0 = 6000)$. In figure 7, the structure factor $S(q)$ is shown for $v_0 n_e = 0, 0.0005, 0.0015$, and 0.0025. The structure factor around the peak is of order $100v_0$ and is much larger than the thermal level.

In figure 8, we display $\phi(\boldsymbol{r}, t)$ and $n_1(\boldsymbol{r}, t)$ at $t = 3000t_0$ for $v_0 n_e = 0.0005$ (left) and 0.0025 (right). As a marked feature for $v_0 n_e = 0.0005$, the cations (anions) are confined in the water-rich (water-poor) regions. Because of the small ion density here, the ions change discontinuously at the interfaces and are homogeneously distributed in the preferred domains. On the other hand, for $v_0 n_e = 0.0025$, the ions are localized near the interfaces. In figure 9, we show cross sections of ϕ, n_1, n_2 (top), and those of f_g, $-f_e$, and $f_g - f_e$ (bottom). We can see electric double layers at the interfaces in accord with the theory [6]. The difference $f_g - f_e$ turns out to be small in steady states. In figure 10, we demonstrate that their space averages nearly coincide at long times. From (2.8) we recognize that the surface tension γ nearly vanishes in steady states.

6. Summary and concluding remarks

In this work, we have presented dynamic equations for binary mixtures containing ions, where the free energy includes the solvation interactions. (i) As the first application, we have calculated the dynamic structure factor $G(q, t)$ in (4.1) in one-

phase states accounting for the ion motions. Its relaxation is slowed down on approaching the spinodal as in (4.12), which occurs at an intermediate wavenumber q_m for $\gamma_p > 1$. Here γ_p is the asymmetry parameter of solvation. It also exhibits a double-exponential relaxation in the long wavelength limit (in dynamic light scattering) as in (4.19). (ii) As the second application, we have numerically demonstrated the emergence of mesophases with the addition of an antagonistic salt, though our simulations are in two dimensions and at the critical composition. We have obtained a dramatic increase of the structure factor $S(q)$ at an intermediate wavenumber in figures 2 and 7 in accord with the experiment of Sadakane *et al* [16, 17]. In these mesophases, the gradient free energy and long-range electrostatic energy are balanced as in figures 5 and 10. We have found that the surface tension vanishes in the mesophase in deep quenching.

The present simulation is still very preliminary and more systematic analysis is needed in future work. In particular, the phase diagram in the parameter space of χ, $\langle\phi\rangle$, and n_e is required. While our simulation captures some salient features of the neutron scattering experiments [16, 17], the calculated structure factor $S(q)$ cannot be compared with the observed intensity quantitatively. There are many parameters in our theory and we cannot judge whether or not our choice in (5.3) is appropriate for the experimental system. In particular, the solvation parameters g_1 and g_2 are not known for mixtures of D_2O and 3MP.

Our simulation suggests that the addition of an antagonistic salt to a binary mixture can decrease the surface tension of a macroscopic liquid–liquid interface even to zero. We may then predict a salt-induced interface instability, leading to emulsification. We also mention measurements of the dynamic scattering, the electric conductivity, and the rheological properties, as new experiments using an antagonistic salt.

Acknowledgments

This work was supported by Grant-in-Aid for Scientific Research on Priority Area 'Soft Matter Physics' from the Ministry of Education, Culture, Sports, Science, and Technology of Japan. Thanks are also given to K Sadakane and H Seto for informative discussions.

References

[1] Levin Y 2002 *Rep. Prog. Phys.* **65** 1577
[2] Holm C, Joanny J F, Kremer K, Netz R R, Reineker P, Seidel C, Vilgis T A and Winkler R G 2004 *Adv. Polym. Sci.* **166** 67
[3] Dobrynin A V and Rubinstein M 2005 *Prog. Polym. Sci.* **30** 1049
[4] Israelachvili J N 1991 *Intermolecular and Surface Forces* (London: Academic)
[5] Onuki A and Kitamura H 2004 *J. Chem. Phys.* **121** 3143
[6] Onuki A 2006 *Phys. Rev.* E **73** 021506
Onuki A 2008 *J. Chem. Phys.* **128** 224704
Onuki A 2009 *Polymer, Liquids and Colloids in Electric Fields: Interfacial Instabilities, Orientation and Phase-Transitions* ed Y Tsori (Singapore: World Scientific)
[7] Marcus G, Samin S and Tsori Y 2008 *J. Chem. Phys.* **129** 061101
[8] Bier M, Zwanikken J and van Roij R 2008 *Phys. Rev. Lett.* **101** 046104
Zwanikken J, de Graaf J, Bier M and van Roij R 2008 *J. Phys.: Condens. Matter* **20** 494238
[9] Ben-Yaakov D, Andelman D, Harries D and Podgornik R 2009 *J. Phys. Chem.* B **10** 6001
[10] Onuki A and Okamoto R 2009 *J. Phys. Chem.* B **113** 3988
[11] Onuki A 2008 *Europhys. Lett.* **82** 58002
[12] Eckfeldt E L and Lucasse W W 1943 *J. Phys. Chem.* **47** 164
Hales B J, Bertrand G L and Hepler L G 1966 *J. Phys. Chem.* **70** 3970
Balevicius V and Fuess H 1999 *Phys. Chem. Chem. Phys.* **1** 1507
Misawa M, Yoshida K, Maruyama K, Munemura H and Hosokawa Y 1999 *J. Phys. Chem. Solids* **60** 1301
[13] Euliss G W and Sorensen C M 1984 *J. Chem. Phys.* **80** 4767
[14] Kostko A F, Anisimov M A and Sengers J V 2004 *Phys. Rev.* E **70** 026118
Wagner M, Stanga O and Schröer W 2004 *Phys. Chem. Chem. Phys.* **6** 580
[15] Jacob J, Anisimov M A, Sengers J V, Oleinikova A, Weingärtner H and Kumar A 2001 *Phys. Chem. Chem. Phys.* **3** 829
[16] Sadakane K, Seto H, Endo H and Shibayama M 2007 *J. Phys. Soc. Japan* **76** 113602
[17] Sadakane K, Onuki A, Nishida K, Koizumi S and Seto H 2009 arXiv:0903.2303v2
[18] Nabutovskii V M, Nemov N A and Peisakhovich Yu G 1980 *Phys. Lett.* A **79** 98
Nabutovskii V M, Nemov N A and Peisakhovich Yu G 1980 *Zh. Eksp. Teor. Fiz.* **79** 2196
Nabutovskii V M, Nemov N A and Peisakhovich Yu G 1980 *Sov. Phys.—JETP* **52** 111 (Engl. Transl.)
Nabutovskii V M, Nemov N A and Peisakhovich Yu G 1985 *Mol. Phys.* **54** 979
[19] Onuki A 2004 *Nonlinear Dielectric Phenomena in Complex Liquids* (*NATO Science Series II* vol 157) ed S J Rzoska (Dordrecht: Kluwer Academic)
[20] Debye P and Kleboth K 1965 *J. Chem. Phys.* **42** 3155
[21] Levin Y and Flores-Mena J E 2001 *Europhys. Lett.* **56** 187
[22] Hung L Q 1980 *J. Electroanal. Chem.* **115** 159
Hung L Q 1983 *J. Electroanal. Chem.* **149** 1
[23] Osakai T and Ebina K 1998 *J. Phys. Chem.* B **102** 5691
[24] Borye V Yu and Erukhimovich I Ya 1988 *Macromolecules* **21** 3240
[25] Joanny J F and Leibler L 1990 *J. Physique* **51** 547
[26] Onuki A 2002 *Phase Transition Dynamics* (Cambridge: Cambridge University Press)
[27] Landau L D and Lifshitz E M 1984 *Electrodynamics of Continuous Media* (Oxford: Pergamon) chapter II
[28] Koga T and Kawasaki K 1993 *Physica* A **196** 389
Koga T and Kawasaki K 1993 *Physica* A **198** 473
[29] Ohta T 2009 *Kinetics of Phase Transitions: Ordering Phenomena and Phase Separation* ed S Puri, CRC Press–Taylor and Francis